Regular Article

MMS

Mathematics and Mechanics of Solids
2020, Vol. 25(7) 1504–1514

DOI: 10.1177/1081286517724607
journals.sagepub.com/home/mms
SAGE

Numerical homogenization of the Eshelby tensor at small strains

Charlotte Kuhn
Computational Mechanics, University of Kaiserslautern, Kaiserslautern, Germany

Ralf Müller
Institute of Applied Mechanics, University of Kaiserslautern, Kaiserslautern, Germany

Markus Klassen
Chair of Structural Analysis and Dynamics, RWTH Aachen, Aachen, Germany

Dietmar Gross
Division of Solid Mechanics, TU Darmstadt, Darmstadt, Germany

Received 12 April 2017; accepted 13 July 2017

Abstract
Numerical homogenization methods, such as the FE^2 approach, are widely used to compute the effective physical properties of microstructured materials. Thereby, the macroscopic material law is replaced by the solution of a microscopic boundary value problem on a representative volume element in conjunction with appropriate averaging techniques. This concept can be extended to configurational or material quantities, like the Eshelby stress tensor, which are associated with configurational changes of continuum bodies. In this work, the focus is on the computation of the macroscopic Eshelby stress tensor within a small-strain setting. The macroscopic Eshelby stress tensor is defined as the volume average of its microscopic counterpart. On the microscale, the Eshelby stress tensor can be computed from quantities known from the solution of the physical microscopic boundary value problem. However, in contrast to the physical quantities of interest, i.e. stress and strain, the Eshelby stress tensor is sensitive to rigid body rotations of the representative volume element. In this work, it is demonstrated how this must be taken into account in the computation of the macroscopic Eshelby stress tensor. The theoretical findings are illustrated by a benchmark simulation and further simulation results indicate the microstructural influence on the macroscopic configurational forces.

Keywords
Numerical homogenization, Eshelby tensor, configurational forces, FE^2, small strain

Corresponding author:
Charlotte Kuhn, Computational Mechanics, University of Kaiserslautern, P.O.B. 3049, 67653 Kaiserslautern, Germany.
Email: chakuhn@rhrk.uni-kl.de

1. Introduction

Homogenization methods are used to predict the macroscopic material response of microstructured materials. Knowing the constitutive behavior in every point of the microstructure, they enable the prediction of the macroscopic material response. If the mechanical response is in the focus, the macroscopic stress–strain relation is to be predicted. It is natural to use averaged microscopic fields as definitions of macroscopic fields. In general, homogenization methods can be subdivided into two types: analytical approaches and numerical homogenization. In approaches of the first type, an analytical solution for a particular microstructural situation is required. Frequently, inclusion situations are addressed with the help of the Eshelby solution [1]. This solution must not be confused with the Eshelby stress tensor from configurational mechanics, which is in the focus of the present investigation. Classical analytical homogenization methods are the dilute distribution scheme, the Mori–Tanaka scheme, the self-consistent scheme, and the differential scheme. All these methods have their advantages and disadvantages; for a more detailed review see, for example, Gross and Seelig [2] and Nemat-Nasser and Hori [3], and the literature cited therein. In general, all analytical homogenization methods must resort to simplifications of the microstructural morphology in order to obtain analytical solutions. To circumvent these simplifying assumptions on the morphology, computational homogenization methods are established, see for example [4, 5]. Frequently, finite element (FE) procedures on both length scales are used. Without claiming completeness we refer the reader to [6–8]. In recent years, a coupling of macroscopic FE solvers with micro solvers based on fast Fourier transform methods has been established, see for example [9–12] and related literature. The key idea of both methods is the attachment of a representative volume element (RVE) to each macroscopic integration point. In so-called FE^2 approaches, the RVE itself is solved by FE. In this investigation, we will focus on this type of computational homogenization, although an adaption to fast Fourier transform based micro solvers is, of course, possible. The two scales are coupled by localization techniques (boundary conditions for the RVE based on macroscopic fields) and averaging procedures (macroscopic quantities as averages of the microscopic quantities).

Independently of the homogenization method or the numerical schemes involved, the focus of homogenization has primarily been on physical quantities, such as stress, strain, and stiffness. However, microstructural defects, such as material interfaces, voids, and cracks, interact with macroscopic defects, such as cracks. An appropriate tool to analyze the behavior of defects and their associated driving forces is the theory of configurational forces, see for example the textbooks [13–17]. A key ingredient of the theory of configurational forces is the Eshelby stress tensor, often called the configurational stress tensor, first introduced in the context of solid mechanics by Eshelby [18, 19]. Owing to the similar structure of the configurational stress to the Maxwell stress of electrostatics, Eshelby called the configurational stress tensor the ‘Maxwell stress tensor of elasticity’.

As the Eshelby or configurational stress tensor satisfies a balance law similar to the one of the physical (Cauchy) stress, attempts to apply homogenization techniques to configurational quantities were undertaken in [20, 21]. Since configurational forces are work conjugated to changes of the reference configuration, it is natural to develop a homogenization technique for configurational quantities in a large deformation context. This was done in the context of hyperelasticity in [20, 21] and for piezoelectric materials at small strains in [22, 23]. In the small deformation regime with linearized strains, some special issues appear, such as the treatment of rigid body rotations of the RVE, the coupling of micro- and macroscale, and the proper definition of a macroscopic Eshelby stress. The aim of this investigation is to shed some light on these issues and to highlight some of the theoretical findings by illustrative examples. Furthermore, the purpose of this investigation is to consider microstructural effects in the computation of macroscopic configurational forces, such as driving forces on cracks and interfaces. The attention is on the small-strain framework. The constitutive relations considered are of linear elastic type. The case of dissipative (history-dependent) materials is deliberately disregarded here, since this topic is subject to ongoing research.

2. Basic equations

As mentioned before, we restrict our attention to a small-strain formulation with linear elastic constitutive relations on the microscale. Thus, the macroscopic behavior is also of linear elastic character. To set up the notation, we will first provide the kinematic, balance, and constitutive equations in the following. As these equations represent a complete set of equations, they are used to solve the field (elasticity) problem on the microscale.

The linearized strain tensor $\boldsymbol{\varepsilon}$ is given by the symmetric part of the displacement gradient

$$\boldsymbol{\varepsilon} = \operatorname{grad}_{\mathrm{s}} \boldsymbol{u} = \frac{1}{2}\left(\operatorname{grad} \boldsymbol{u} + (\operatorname{grad} \boldsymbol{u})^{\mathrm{T}}\right) , \tag{1}$$

where $\boldsymbol{u}$ is the displacement field and the subscript s indicates the symmetric part of the gradient. The antisymmetric, rotational, part $\boldsymbol{R}$ of the displacement gradient is given by

$$\boldsymbol{R} = \operatorname{grad} \boldsymbol{u} - \boldsymbol{\varepsilon} = \frac{1}{2}\left(\operatorname{grad} \boldsymbol{u} - (\operatorname{grad} \boldsymbol{u})^{\mathrm{T}}\right) . \tag{2}$$

The physical (Cauchy) stress tensor $\boldsymbol{\sigma}$ satisfies the equilibrium condition

$$\operatorname{div} \boldsymbol{\sigma} + \boldsymbol{f} = \boldsymbol{0} , \tag{3}$$

with physical volume forces $\boldsymbol{f}$. In homogenization schemes, the RVE must be small compared with a characteristic size of the macroscopic structure. Thus, volume forces are frequently neglected, i.e. $\boldsymbol{f} = \boldsymbol{0}$. In this case, the Cauchy stress is a conserved quantity, as it satisfies

$$\operatorname{div} \boldsymbol{\sigma} = \boldsymbol{0} . \tag{4}$$

For a discussion on conservation laws in elasticity, the reader is referred to Kienzler and Herrmann [16] and Buggisch et al. [24]. The set of equations is completed by the constitutive relation

$$\boldsymbol{\sigma} = \mathbb{C}\boldsymbol{\varepsilon} , \tag{5}$$

where $\mathbb{C}$ is the fourth-order elastic stiffness tensor. Using the strain energy density ψ, the constitutive law can be expressed as

$$\boldsymbol{\sigma} = \frac{\partial \psi}{\partial \boldsymbol{\varepsilon}} , \tag{6}$$

where the strain energy density ψ of a linear elastic material is given by the quadratic form

$$\psi = \frac{1}{2}\boldsymbol{\varepsilon} : (\mathbb{C}\boldsymbol{\varepsilon}) . \tag{7}$$

Following Eshelby [19], one can compute the gradient of the strain energy density ψ to derive the configurational force balance

$$\operatorname{div} \boldsymbol{\Sigma} + \boldsymbol{g} = \boldsymbol{0} , \tag{8}$$

where the Eshelby stress tensor $\boldsymbol{\Sigma}$ is given by

$$\boldsymbol{\Sigma} = \psi \boldsymbol{1} - (\operatorname{grad} \boldsymbol{u})^{\mathrm{T}} \boldsymbol{\sigma} , \tag{9}$$

and

$$\boldsymbol{g} = - (\operatorname{grad} \boldsymbol{u})^{\mathrm{T}} \boldsymbol{f} - \left.\frac{\partial \psi}{\partial x}\right|_{\text{expl.}} \tag{10}$$

is the configurational volume force. To obtain (8) from the gradient of ψ, the physical equilibrium (3) and the kinematic relation (1) must be used in conjunction with the constitutive relation (6). For the derivation of the configurational force balance, the reader is referred to [13–17]. Even in the case of vanishing physical volume forces $\boldsymbol{f}$, the configurational volume force $\boldsymbol{g}$ contains a term sensitive to heterogeneities, i.e.

$$\boldsymbol{g} = - \left.\frac{\partial \psi}{\partial x}\right|_{\text{expl.}} . \tag{11}$$

It is emphasized here, that (11) also includes the case of interfaces between two phases with different elastic properties. In this case, the explicit dependency of the strain energy density ψ is characterized by a Heaviside step function, resulting in a configurational volume force localized at the interface, which is described by a Dirac delta distribution. This topic is not elaborated in detail here, but re-examined in the numerical examples.

The implementation of the configurational force balance as a post-processing step in the FE method is documented in several publications. Without claiming completeness, we cite here [25–33].

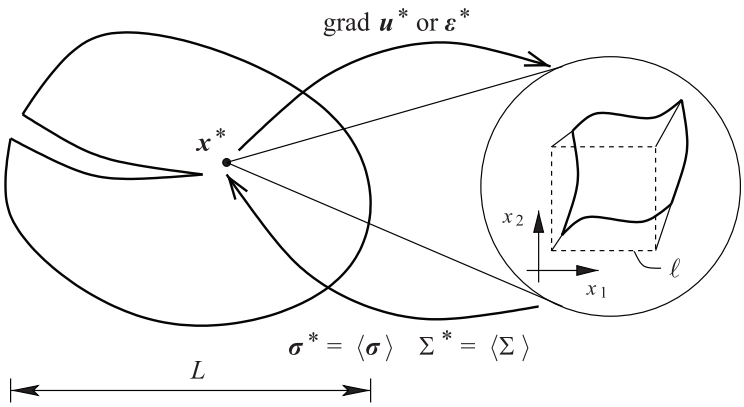

Figure 1. Computational homogenization setup. Representative volume element (RVE, right) attached to macroscale integration point $\boldsymbol{x}^*$ (left).

3. FE^2 approach

3.1. Scale transition of physical quantities

To compute the residuals of the macroscale FE problem, a constitutive relation between the strains and stresses must be evaluated in every integration point $\boldsymbol{x}^*$ of the macroscale problem. Within the FE^2 homogenization scheme, which is utilized in this work, a microscale boundary value problem is formulated for every integration point $\boldsymbol{x}^*$ to incorporate the effects of the heterogeneous micro structure in the computation of the macroscopic material behavior, see Figure 1. The microscale problem is formulated for an RVE. On the one hand, the RVE must be small compared to the size of the macroscopic problem ($\ell \ll L$) in order to represent a single macroscopic point with constant stresses and strains. On the other hand, it must be large enough to be representative of the heterogeneous microstructure.

According to Hill's principle [34], the connection between macroscopic variables (denoted $(\cdot)^*$ in the following) and the respective quantities on the microscale should be formulated such that the macroscopic quantities depend solely on surface data of the RVE. If there are no displacement jumps in the heterogeneous microscale problem, the volume average of the strain in an RVE $\langle \boldsymbol{\varepsilon} \rangle$ can be computed solely from the surface displacements of the RVE, i.e.

$$\langle \boldsymbol{\varepsilon} \rangle = \frac{1}{V_{\mathrm{RVE}}} \int_{V_{\mathrm{RVE}}} \boldsymbol{\varepsilon} \, \mathrm{d}V = \frac{1}{2V_{\mathrm{RVE}}} \int_{\partial V_{\mathrm{RVE}}} (\boldsymbol{u} \otimes \boldsymbol{n} + \boldsymbol{n} \otimes \boldsymbol{u}) \, \mathrm{d}A \,, \tag{12}$$

where V_{RVE} is the volume, $\partial V_{\mathrm{RVE}}$ is the boundary, and $\boldsymbol{n}$ is the outer normal vector of the RVE. Thus, it is feasible to assume

$$\boldsymbol{\varepsilon}^* = \langle \boldsymbol{\varepsilon} \rangle \tag{13}$$

for the scale transition of the infinitesimal strain tensor.

A macroscopic stress tensor derived from surface tractions $\boldsymbol{t}$ at the RVE boundary is given by

$$\boldsymbol{\sigma}^* = \frac{1}{V_{\mathrm{RVE}}} \int_{\partial V_{\mathrm{RVE}}} \boldsymbol{t} \otimes \boldsymbol{x} \, \mathrm{d}A \,. \tag{14}$$

In the absence of volume forces, this is equivalent to the volume average of the microscopic stress tensor, i.e.

$$\boldsymbol{\sigma}^* = \frac{1}{V_{\mathrm{RVE}}} \int_{\partial V_{\mathrm{RVE}}} \boldsymbol{t} \otimes \boldsymbol{x} \, \mathrm{d}A = \frac{1}{V_{\mathrm{RVE}}} \int_{V_{\mathrm{RVE}}} \boldsymbol{\sigma} \, \mathrm{d}V = \langle \boldsymbol{\sigma} \rangle \,. \tag{15}$$

The macroscopic quantities defined in this way satisfy the Hill–Mandel condition

$$\boldsymbol{\sigma}^* : \boldsymbol{\varepsilon}^* = \langle \boldsymbol{\sigma} : \boldsymbol{\varepsilon} \rangle \,. \tag{16}$$

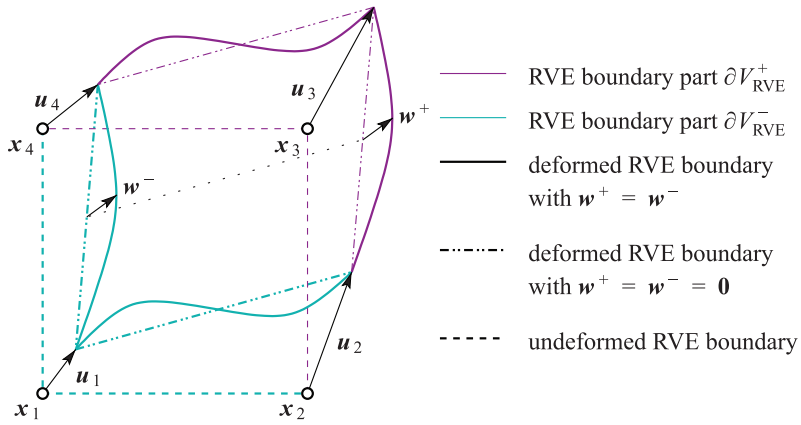

Figure 2. Two-dimensional RVE with periodic boundary conditions.

3.2. RVE boundary conditions

At the microscopic level, the following linear elastic problem has to be solved in the domain of the RVE:

$$\mathbf{0} = \operatorname{div} \boldsymbol{\sigma}\,, \tag{17}$$

$$\boldsymbol{\sigma} = \mathbb{C}(\boldsymbol{x})\boldsymbol{\varepsilon}\,, \tag{18}$$

$$\boldsymbol{\varepsilon} = \frac{1}{2}\left(\operatorname{grad}\boldsymbol{u} + (\operatorname{grad}\boldsymbol{u})^{\mathrm{T}}\right)\,. \tag{19}$$

Additionally, boundary conditions must be specified. In a strain-driven approach, which is followed here, the boundary conditions are derived from the macroscopic displacement field.

Within the first-order homogenization scheme, which is utilized here, the displacement field in the RVE is given by

$$\boldsymbol{u}(\boldsymbol{x}) = \boldsymbol{u}^* + \operatorname{grad}\boldsymbol{u}^*\,\boldsymbol{x} + \boldsymbol{w}(\boldsymbol{x})\,, \tag{20}$$

where $\boldsymbol{u}^*$ and $\operatorname{grad}\boldsymbol{u}^*$ are the displacement and the displacement gradient at the macroscopic integration point $\boldsymbol{x}^*$, to which the RVE is attached, and $\boldsymbol{w}$ are possible fluctuations on the microscale. For this fluctuation field, assumption (13) implies that

$$\int_{V_{\mathrm{RVE}}} \operatorname{grad}_{\mathrm{s}}\boldsymbol{w}\,\mathrm{d}V = \frac{1}{2}\int_{\partial V_{\mathrm{RVE}}} (\boldsymbol{w}\otimes\boldsymbol{n} + \boldsymbol{n}\otimes\boldsymbol{w})\,\mathrm{d}A = \mathbf{0}\,. \tag{21}$$

This constraint is satisfied, if $\boldsymbol{w} = \mathbf{0}$ on $\partial V_{\mathrm{RVE}}$, i.e. prescribed linear displacements on the RVE boundary, or in the more general case of periodic boundary conditions, where

$$\boldsymbol{w}^- = \boldsymbol{w}^+ \tag{22}$$

on opposite sides of a parallelepiped RVE, as depicted in Figure 2 for the 2D case. Owing to the periodicity condition (22), a non-vanishing fluctuation at a corner of the RVE would involve an identical fluctuation at all RVE corners. This would only induce a rigid body translation of the entire RVE, which does not influence the strain and stress states inside the RVE. Thus, without loss of generality, it may be assumed that the fluctuations vanish at the corners of the RVE.

Using equation (2), the microscale displacement field (20) may be split into

$$\boldsymbol{u}(\boldsymbol{x}) = (\boldsymbol{u}^* + \boldsymbol{R}^*\boldsymbol{x}) + (\boldsymbol{\varepsilon}^*\boldsymbol{x} + \boldsymbol{w}(\boldsymbol{x}))\,, \tag{23}$$

where the first part is a pure rigid body motion of the RVE. Since

$$\begin{aligned}\boldsymbol{\varepsilon} = \operatorname{grad}_{\mathrm{s}}\boldsymbol{u} &= \frac{1}{2}\left(\boldsymbol{R}^* + \boldsymbol{R}^{*\mathrm{T}}\right) + \frac{1}{2}\left(\boldsymbol{\varepsilon}^* + \boldsymbol{\varepsilon}^{*\mathrm{T}}\right) + \operatorname{grad}_{\mathrm{s}}\boldsymbol{w}\\ &= \boldsymbol{\varepsilon}^* + \operatorname{grad}_{\mathrm{s}}\boldsymbol{w}\,,\end{aligned} \tag{24}$$

the rigid body motion induced by $\boldsymbol{u}^*$ and $\boldsymbol{R}^*$ does not contribute to the strain and stress states in the RVE and is often omitted in the formulation of the RVE boundary conditions. We will do so for the macroscopic displacement $\boldsymbol{u}^*$, but we will now consider more closely the two cases where the displacements of the corners of the RVE are prescribed on the basis of $\operatorname{grad}\boldsymbol{u}^*$ (containing the macroscopic rotation $\boldsymbol{R}^*$) and on the basis of $\boldsymbol{\varepsilon}^*$, respectively. Thus, the displacements of the RVE corners $\boldsymbol{x}_K$ are prescribed as

$$\boldsymbol{u}_{K|\nabla u} = \operatorname{grad}\boldsymbol{u}^*\,\boldsymbol{x}_K \qquad \text{and} \qquad \boldsymbol{u}_{K|\varepsilon} = \boldsymbol{\varepsilon}^*\,\boldsymbol{x}_K \tag{25}$$

in the two alternative scenarios. Here and in the following, the subscripts $(\cdot)_{\nabla u}$ and $(\cdot)_\varepsilon$ are used to differentiate between these two cases. The so-prescribed corner displacements differ by the macroscale rotation $\boldsymbol{R}^*$ of the RVE corner positions $\boldsymbol{x}_K$, i.e.

$$\boldsymbol{u}_{K|\nabla u} - \boldsymbol{u}_{K|\varepsilon} = (\operatorname{grad}\boldsymbol{u}^* - \boldsymbol{\varepsilon}^*)\,\boldsymbol{x}_K = \boldsymbol{R}^*\,\boldsymbol{x}_K\,. \tag{26}$$

Suppose that

$$\boldsymbol{u}_{\nabla u}(\boldsymbol{x}) = \operatorname{grad}\boldsymbol{u}^*\boldsymbol{x} + \boldsymbol{w}(\boldsymbol{x}) \tag{27}$$

is a solution to the linear RVE problem (17) to (19) with corner displacements according to $(25)_1$ and periodic boundary conditions (22). Then

$$\boldsymbol{u}_\varepsilon(\boldsymbol{x}) = \boldsymbol{\varepsilon}^*\boldsymbol{x} + \boldsymbol{w}(\boldsymbol{x}) = \boldsymbol{u}_{\nabla u}(\boldsymbol{x}) - \boldsymbol{R}^*\boldsymbol{x} \tag{28}$$

does also solve the system of equations (17) to (19), since

$$\boldsymbol{\varepsilon}_{\nabla u} = \boldsymbol{\varepsilon}^* + \operatorname{grad}_{\mathrm{s}}\boldsymbol{w} = \boldsymbol{\varepsilon}_\varepsilon\,. \tag{29}$$

Furthermore, $\boldsymbol{u}_\varepsilon(\boldsymbol{x})$ satisfies the corner displacement constraints $(25)_2$.

Since the microscopic strain fields $\boldsymbol{\varepsilon}_{\nabla u}$ and $\boldsymbol{\varepsilon}_\varepsilon$ are the same, the two approaches are equivalent and both are feasible to compute the macroscopic stress $\boldsymbol{\sigma}^* = \langle\boldsymbol{\sigma}\rangle$.

3.3. Averaged Eshelby stress tensor

Now, besides the macroscopic stress $\boldsymbol{\sigma}^*$, a macroscopic Eshelby stress tensor $\boldsymbol{\Sigma}^*$ shall be provided for the macroscale. For a non-graded material, where the material properties inside the RVE do not explicitly depend on the coordinate $\boldsymbol{x}$, the macroscopic Eshelby stress tensor may be defined as the volume average of the Eshelby stress tensor in the RVE, i.e.

$$\boldsymbol{\Sigma}^* = \langle\boldsymbol{\Sigma}\rangle = \frac{1}{V_{\mathrm{RVE}}}\int_{V_{\mathrm{RVE}}}\boldsymbol{\Sigma}\,\mathrm{d}V = \frac{1}{V_{\mathrm{RVE}}}\int_{V_{\mathrm{RVE}}}\left(\psi\mathbf{1} + (\operatorname{grad}\boldsymbol{u})^{\mathrm{T}}\,\boldsymbol{\sigma}\right)\mathrm{d}V\,. \tag{30}$$

While the strains $\boldsymbol{\varepsilon}$ and stresses $\boldsymbol{\sigma}$ and, consequently, the energy density ψ are the same for both boundary conditions considered, the displacement gradients $\operatorname{grad}\boldsymbol{u}_{\nabla u}$ and $\operatorname{grad}\boldsymbol{u}_\varepsilon$ within the RVE differ by the macroscopic rotation $\boldsymbol{R}^*$, i.e.

$$\operatorname{grad}\boldsymbol{u}_{\nabla u} - \operatorname{grad}\boldsymbol{u}_\varepsilon = (\operatorname{grad}\boldsymbol{u}^* + \operatorname{grad}(\boldsymbol{w})) - (\boldsymbol{\varepsilon}^* + \operatorname{grad}(\boldsymbol{w})) = \boldsymbol{R}^*\,. \tag{31}$$

Accordingly, the Eshelby stress tensors $\boldsymbol{\Sigma}_{\nabla u}$ and $\boldsymbol{\Sigma}_\varepsilon$ on the microscale differ, leading to different values for the averaged Eshelby stress $\langle\boldsymbol{\Sigma}\rangle$. Regarding the microscale problem, both $\boldsymbol{\Sigma}_{\nabla u}$ and $\boldsymbol{\Sigma}_\varepsilon$ are meaningful and can be used to evaluate the configurational forces acting within the RVE. However, since the rotational part of $\operatorname{grad}\boldsymbol{u}^*$ is missing in the microscale problem solution $\boldsymbol{u}_\varepsilon$, only $\boldsymbol{\Sigma}^*_{\nabla u} = \langle\boldsymbol{\Sigma}_{\nabla u}\rangle$ is physically meaningful on the macroscale. This might suggest that one must consider the microscale problem with $\operatorname{grad}\boldsymbol{u}^*$-boundary conditions according to $(25)_1$, to compute a meaningful averaged Eshelby stress tensor. However, this is not the case, since the wrong, unphysical averaged Eshelby stress $\boldsymbol{\Sigma}^*_\varepsilon = \langle\boldsymbol{\Sigma}_\varepsilon\rangle$ can be corrected at the macroscale by means of the relation

$$\begin{aligned}
\boldsymbol{\Sigma}^*_{\nabla u} = \langle\boldsymbol{\Sigma}_{\nabla u}\rangle &= \frac{1}{V_{\mathrm{RVE}}}\int_{V_{\mathrm{RVE}}}\left(\psi\mathbf{1} - (\operatorname{grad}\boldsymbol{u}_{\nabla u})^{\mathrm{T}}\,\boldsymbol{\sigma}\right)\mathrm{d}V \\
&= \frac{1}{V_{\mathrm{RVE}}}\left[\int_{V_{\mathrm{RVE}}}\left(\psi\mathbf{1} - (\operatorname{grad}\boldsymbol{u}_\varepsilon)^{\mathrm{T}}\,\boldsymbol{\sigma}\right)\mathrm{d}V - \int_{V_{\mathrm{RVE}}}\boldsymbol{R}^{*\mathrm{T}}\boldsymbol{\sigma}\,\mathrm{d}V\right] \\
&= \langle\boldsymbol{\Sigma}_\varepsilon\rangle - \boldsymbol{R}^{*\mathrm{T}}\langle\boldsymbol{\sigma}\rangle = \boldsymbol{\Sigma}^*_\varepsilon - \boldsymbol{R}^{*\mathrm{T}}\boldsymbol{\sigma}^*\,.
\end{aligned} \tag{32}$$

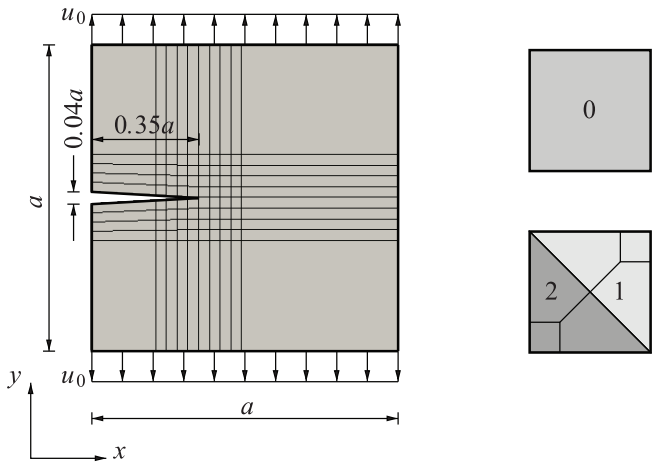

Figure 3. Setup for the computation of configurational forces at a crack tip under mode I loading. Left: geometry, mesh, and loading conditions. Top right: homogeneous representative volume element. Bottom right: inhomogeneous representative volume element.

This is worthy of note because usually periodic boundary conditions for the RVE are defined on the basis of $\boldsymbol{\varepsilon}^*$ rather than on $\operatorname{grad}\boldsymbol{u}^*$. With the correction term $\boldsymbol{R}^{*\mathrm{T}}\boldsymbol{\sigma}^*$ it is possible to obtain the correct averaged Eshelby stress tensor from the microscale without having to change the FE implementation on the microscale from $\boldsymbol{\varepsilon}^*$-boundary conditions to $\operatorname{grad}\boldsymbol{u}^*$-boundary conditions.

Alternatively to equation (30), the macroscopic Eshelby stress tensor may be defined solely on the basis of macroscopic quantities, i.e.

$$\tilde{\boldsymbol{\Sigma}}^* = \psi^*\mathbf{1} - (\operatorname{grad}\boldsymbol{u}^*)^{\mathrm{T}}\boldsymbol{\sigma}^* . \tag{33}$$

Using the Hill–Mandel relation (16), the microscale displacement field (27), and the scale transition (15) for the stress tensor, the difference to the averaged Eshelby stress tensor is

$$\tilde{\boldsymbol{\Sigma}}^* - \langle\boldsymbol{\Sigma}_{\nabla u}\rangle = \frac{1}{V_{\mathrm{RVE}}}\int_{V_{\mathrm{RVE}}} (\operatorname{grad}\boldsymbol{w})^{\mathrm{T}}\boldsymbol{\sigma}\,\mathrm{d}V . \tag{34}$$

As shown by Ricker et al. [20, 21] for the case of finite deformations, this term does not vanish in general. Ricker et al. [20, 21] also argue, by means of a Hill–Mandel type relation for the Eshelby stress tensor, that the averaged Eshelby stress tensor is to be preferred as a macroscopic configurational stress tensor. More specifically, the averaged Eshelby stress tensor satisfies the Hill–Mandel relation for the configurational work without further ado, whereas additional internal terms arise in this relation if the macroscopic Eshelby stress tensor is computed on the macroscale from homogenized quantities. Therefore, the latter alternative definition (34) will not be considered in the following numerical examples.

4. Numerical examples

4.1. Configurational force at a crack tip

4.1.1. Homogeneous RVE. This first example is to benchmark the FE^2 implementation in a simulation with a homogeneous RVE, as depicted in the top right panel of Figure 3. In this case, the FE^2 simulation should give the same results as a regular FE simulation with a homogeneous material. Furthermore, the necessity to consider the rotational part of the displacement gradient in the computation of the averaged Eshelby stress tensor $\boldsymbol{\Sigma}^* = \langle\boldsymbol{\Sigma}\rangle$ will be emphasized.

The geometry of the problem and the loading scenario, as well as the discretization of the macroscale problem, are shown in the left panel of Figure 3, where $a = 10\,\mathrm{cm}$ and $u_0 = 1\,\mathrm{mm}$. A plane strain state is assumed in this and all following simulations. The elastic material parameters of the homogeneous RVE are $E_0 = 70\,\mathrm{GPa}$ (Young's modulus) and $\nu = 0.3$ (Poisson's ratio), and the RVE is discretized with only one element.

The plots in Figure 4 show the nodal configurational forces computed from $\boldsymbol{\Sigma}^*_{\varepsilon} = \langle\boldsymbol{\Sigma}_{\varepsilon}\rangle$ (left panel), and $\boldsymbol{\Sigma}^*_{\nabla u} = \langle\boldsymbol{\Sigma}_{\nabla u}\rangle$ (right panel), respectively. In the considered scenario, a significant configurational force should

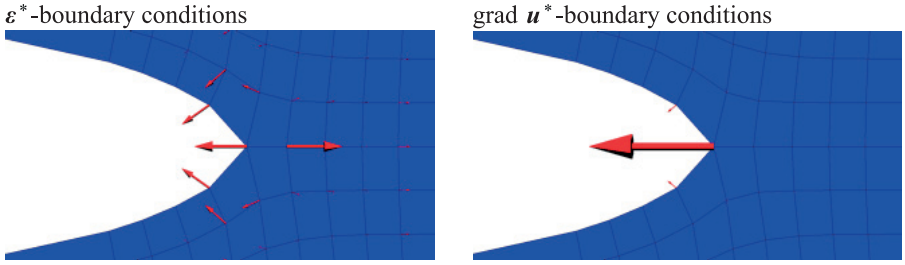

Figure 4. Results of the simulation with homogeneous representative volume element. Nodal configurational forces around the crack tip computed from (left) $\boldsymbol{\Sigma}^*_{\varepsilon} = \langle \boldsymbol{\Sigma}_{\varepsilon} \rangle$ and (right) $\boldsymbol{\Sigma}^*_{\nabla u} = \langle \boldsymbol{\Sigma}_{\nabla u} \rangle$. Deformation exaggerated by a factor of ten.

only be present at the crack tip. However, there are significant configurational forces at some nodes around the notch tip in the left plot of Figure 4, where the configurational forces are computed from $\boldsymbol{\Sigma}^*_{\varepsilon}$. Unlike spurious configurational forces, which indicate a numerical error of the FE approximation, these nodal configurational forces cannot be avoided by a refinement of the mesh. The actual reason for the appearance of these configurational forces is the fact that the rotational part of the macroscopic displacement gradient is missing in the computation of the Eshelby stress tensor $\boldsymbol{\Sigma}_{\varepsilon}$ on the microscale. The right plot of Figure 4 shows the configurational forces computed from $\boldsymbol{\Sigma}^*_{\nabla u}$. Even though the same mesh was used in the simulation, a significant configurational force does now only appear at the crack tip, as expected. The small spurious configurational forces at nodes in the vicinity of the crack tip indicate the numerical error in the computed mechanical fields, see also [25, 26, 28].

4.1.2. Inhomogeneous RVE. The same macroscale problem is now considered, but with an inhomogeneous microstructure represented by the RVE in the bottom right panel of Figure 3, where $E_1 = 10\,\text{GPa}$, $E_2 = 300\,\text{GPa}$, and $\nu = 0.3$ for both material phases. Since the results from the previous simulation have demonstrated that configurational forces computed on the basis of $\boldsymbol{\Sigma}^*_{\varepsilon}$ do not have a clear physical meaning on the macroscale, here the configurational forces are here computed on the basis of $\boldsymbol{\Sigma}^*_{\nabla u}$, or, alternatively, by using the correction of $\boldsymbol{\Sigma}^*_{\varepsilon}$ proposed in (32).

Figure 5 shows contour plots of the computed displacement fields. Owing to the inclined orientation of the material interface in the RVE with respect to the crack ligament and the direction of loading, the macroscopic material behavior is anisotropic and the structure deforms asymmetrically. The configurational force at the crack tip, which is indicated by the arrows in Figure 5, is

$$\boldsymbol{G}_{\text{ct}} = \begin{bmatrix} -4952.03 \\ -259.42 \end{bmatrix} \text{N}\,. \tag{35}$$

The non-vanishing component in the y-direction indicates the influence of the inhomogeneous microstructure on the macroscopic configurational force.

4.2. Configurational forces at a macroscopic material interface

A macroscopically heterogeneous structure, as depicted in the left panel of Figure 6, where $a = 10\,\text{cm}$, is considered in this last example. The orientation of the layered RVE representing the microstructure in the upper and lower parts of the structure is rotated by 90°. As in the previous simulations, the material data are $E_0 = 70\,\text{GPa}$, $E_1 = 10\,\text{GPa}$, and $\nu = 0.3$ for both layers. The structure is loaded by a displacement load of $u_0 = 1\,\text{mm}$ at the upper edge. Note that the simulation setup is chosen such that the macroscopic strain in the x-direction is identical in both parts of the structure, and thus a homogeneous deformation state without any distortion at the interface is observed in the structure. Therefore, the rather coarse discretization of the macroscopic structure with only 4×8 elements is sufficient for this simulation.

The plot on the right-hand side of Figure 6 shows the nodal configurational forces computed from $\boldsymbol{\Sigma}^*_{\nabla u}$. As expected, configurational forces perpendicular to the boundary and perpendicular to the interface appear at the boundary and interface nodes, respectively. Also, as expected, the configurational forces at the interface point from the (in y-direction) stiffer to the (in y-direction) more compliant material. With the macroscopic Eshelby

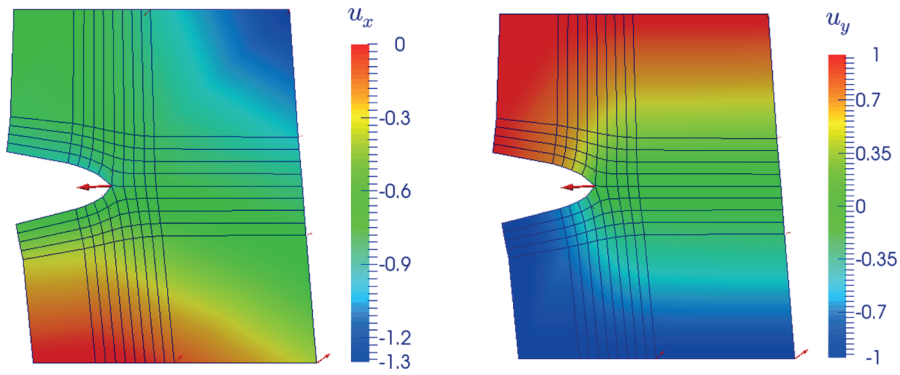

Figure 5. Results of the simulation with inhomogeneous representative volume element. Contour plots of the displacement in (left) x-direction and (right) y-direction in millimeters on the deformed configuration (deformation exaggerated by a factor of ten), and configurational forces (arrows).

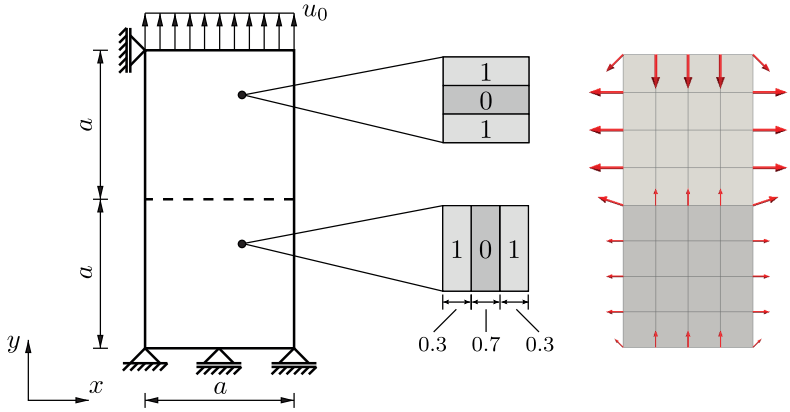

Figure 6. Left: simulation setup for plate with macroscopic interface modeled through differently oriented representative volume elements in the lower and upper parts of the structure. Right: nodal configurational forces (arrows) on the deformed mesh. Deformation exaggerated by a factor of 20.

stress tensors $\boldsymbol{\Sigma}^*_{\text{top}}$ and $\boldsymbol{\Sigma}^*_{\text{bot}}$ in the upper and lower parts of the structure and the unit vector $\boldsymbol{n}_y$ in y-direction, the computed configurational traction at the interface is

$$\left(\boldsymbol{\Sigma}^*_{\text{top}} - \boldsymbol{\Sigma}^*_{\text{bot}}\right)\boldsymbol{n}_y = \begin{bmatrix} 0 \\ 0.2081 \end{bmatrix} \text{MPa}, \tag{36}$$

which is virtually identical to the analytic solution for this problem.

5. Conclusions

To incorporate microstructural effects in the evaluation of configurational forces acting on material inhomogeneities, a method to compute an effective macroscopic Eshelby stress tensor within a multiscale FE^2 framework has been examined. Within this work, the effective macroscopic Eshelby stress tensor is defined as the volume average of the microscopic Eshelby stress tensor over the volume of the respective RVE. When the boundary conditions for the RVEs are formulated based on the macroscopic strain tensor, as is often done in the considered small-strain, linear elastic context, the rotational part of the displacement gradient is not present on the microscale. This is sufficient for the computation of the (physical) Cauchy stress tensor as well as the elastic stiffness tensor, since both are not affected by rigid body rotations. However, when computing the microscopic displacement gradient within such a framework, the rotational part stems exclusively from the fluctuation field, and the volume average cannot recover the macroscopic displacement gradient. Instead, the volume average of the displacement gradient is equal to the macroscopic strain tensor. Since the (configurational) Eshelby

stress tensor depends explicitly on the displacement gradient, this inconsistency in the micro-to-macro transition of the displacement gradient is directly passed on to the scale transition of the Eshelby stress tensor. As demonstrated by the first numerical example, macroscopic configurational forces computed on the basis of the volume average of the microscopic Eshelby stress tensor do not have a clear physical meaning, when the RVE boundary conditions are defined by the macroscopic strain tensor.

Two methods have been suggested to obtain a consistent averaged Eshelby stress tensor, which enables the computation of physically reasonable configurational forces on the macroscale. The first method is to define the RVE boundary conditions on the basis of the macroscopic displacement gradient. By doing so, the volume average of the microscopic displacement gradient recovers the macroscopic displacement gradient, i.e. the aforementioned inconsistency is removed. The rotational part of the macroscopic displacement gradient is no longer missing on the microscale, and the volume average of the Eshelby stress tensor yields physically reasonable configurational forces on the macroscale. If it is not possible to change the definition of the RVE boundary conditions in an FE implementation, the macroscopic Eshelby stress tensor, computed with RVE boundary conditions defined by the macroscopic strain tensor, can alternatively be corrected on the macroscale by subtracting a tensor formed by the transpose of the macroscopic rotation and the macroscopic Cauchy stress tensor. It has been shown that both of these methods yield exactly the same results. The first numerical example demonstrates that physically sound configurational forces can be computed if the rotational part of the macroscopic displacement gradient is incorporated in the computation of the effective Eshelby stress tensor. By means of further numerical examples, it is demonstrated that the homogenization approach is also feasible to compute the deflection of the configurational force at a crack tip due to an inhomogeneous microstructure, and configurational tractions at a macroscopic material interface.

Further analysis of the differences of the averaged Eshelby stress tensor from the alternative definition of a macroscopic Eshelby stress based solely on macroscopic quantities, as well as an extension to dissipative materials where gradients of the internal variables enter the configurational force balance, are part of ongoing research.

Funding

The author(s) disclosed receipt of the following financial support for the research, authorship, and/or publication of this article: This work was supported by the German Federal Ministry of Education and Research (Grant Number 05M2013 ‘Adaptive approximation methods for the multi-scale simulation of the nonlinear behavior of composites’ (MuSiKo)).

References

[1] Eshelby JD. The determination of the elastic field of an ellipsoidal inclusion and related problems. *Proc R Soc Lond A* 1957; 241: 376–396.

[2] Gross D, and Seelig T. *Fracture mechanics: with an introduction to micromechanics*. Heidelberg: Springer Science & Business Media, 2011.

[3] Nemat-Nasser S, and Hori M. *Micromechanics: overall properties of heterogeneous materials*. Amsterdam: North Holland, 1993.

[4] Mishnaevsky Jr LL. *Computational mesomechanics of composites: numerical analysis of the effect of microstructures of composites of strength and damage resistance*. Chichester: JohnWiley & Sons, 2007.

[5] Zohdi TI, and Wriggers P. *An introduction to computational micromechanics*. Berlin: Springer Science & Business Media, 2008.

[6] Miehe C, Schotte J, and Schröder J. Computational micro–macro transitions and overall moduli in the analysis of polycrystals at large strains. *Comput Mater Sci* 1999; 16(1): 372–382.

[7] Kouznetsova V, Brekelmans W, and Baaijens F. An approach to micro-macro modeling of heterogeneous materials. *Computational Mech* 2001; 27(1): 37–48.

[8] Miehe C. Computational micro-to-macro transitions for discretized micro-structures of heterogeneous materials at finite strains based on the minimization of averaged incremental energy. *Comput Methods Appl Mech Eng* 2003; 192(5): 559–591.

[9] Moulinec H and Suquet P. A fast numerical method for computing the linear and nonlinear mechanical properties of composites. *CR Acad Sci, Ser IIb: Mec, Phys, Chim, Astron* 1994; 318(11): 1417–1423.

[10] Moulinec H, and Suquet P. A numerical method for computing the overall response of nonlinear composites with complex microstructure. *Comp Methods Appl Mech Eng* 1998; 157(1–2): 69–94.

[11] Michel J, Moulinec H, and Suquet P. Effective properties of composite materials with periodic microstructure: a computational approach. *Comp Methods Appl Mech Eng* 1999; 172(1–4): 109–143.

[12] Spahn J, Andrä H, Kabel M, et al. A multiscale approach for modeling progressive damage of composite materials using fast Fourier transforms. *Comp Methods Appl Mech Eng* 2014; 268: 871–883.

[13] Gurtin ME. The nature of configurational forces. *Arch Ration Mech Anal* 1995; 131: 67–100.

[14] Gurtin ME. *Configurational forces as basic concepts of continuum physics*. Berlin: Springer, 2000.
[15] Maugin GA. *Material inhomogeneities in elasticity*. London: Chapman & Hall, 1993.
[16] Kienzler R, and Herrmann G. *Mechanics in material space*. New York: Springer, 2000.
[17] Maugin GA. *Configurational forces: thermomechanics, physics, mathematics, and numerics*. Boca Raton: CRC Press, 2016.
[18] Eshelby JD. The force on an elastic singularity. *Phil Trans R Soc Lond A* 1951; 244: 87–112.
[19] Eshelby JD. Energy relations and the energy-momentum tensor in continuum mechanics. In: Kanninen MF (ed.) *Inelastic behaviour of solids*. New York: McGraw Hill, 1970, 77–115.
[20] Ricker S, Mergheim J, and Steinmann P. On the multiscale computation of defect driving forces. *Int J Multiscale Comput Eng* 2009; 7(5): 457–474.
[21] Ricker S, Mergheim J, Steinmann P, et al. A comparison of different approaches in the multi-scale computation of configurational forces. *Int J Fract* 2010; 166(1–2): 203–214.
[22] Khalaquzzaman M, Ricker S, and Müller R. Computational homogenization of piezoelectric materials using FE2. *Proc Appl Math Mech* 2010; 10(1): 417–418.
[23] Khalaquzzaman M, Xu B, Ricker S, et al. Computational homogenization of piezoelectric materials using FE2 to determine configurational forces. *Tech Mech* 2012; 32(1): 21–37.
[24] Buggisch H, Gross D, and Krüger KH. Einige Erhaltungssätze der Kontinuumsmechanik vom JIntegral Typ. *Ing Arch* 1981; 50: 103–111.
[25] Mueller R, Kolling S, and Gross D. On configurational forces in the context of the finite element method. *Int J Numer Methods Eng* 2002; 53: 1557–1574.
[26] Mueller R, and Maugin G. On material forces and finite element discretizations. *Comput Mech* 2002; 29(1): 52–60.
[27] Gross D, Kolling S, Mueller R, et al. Configurational forces and their application in solid mechanics. *Eur J Mech A Solids* 2003; 22: 669–692.
[28] Mueller R, Gross D, and Maugin G. Use of material forces in adaptive finite element methods. *Comput Mech* 2004; 33: 421–434.
[29] Steinmann P. Application of material forces to hyperelastic fracture mechanics. I. Continuum mechanical setting *Int J Solids Struct* 2000; 37(48–50): 7371–7391.
[30] Steinmann P, Ackermann D, and Barth FJ. Application of material forces to hyperelastic fracture mechanics. II. Computational setting *Int J Solids Struct* 2001; 38(32–33): 5509–5526.
[31] Miehe C and Gürses E. A robust algorithm for configurational-force-driven brittle crack propagation with R-adaptive mesh alignment. *Int J Numer Methods Eng* 2007; 72(2): 127–155.
[32] Miehe C, Gürses E, and Birkle M. A computational framework of configurational-force-driven brittle fracture based on incremental energy minimization. *Int J Fract* 2007; 145(4): 245–259.
[33] Gürses E, and Miehe C. A computational framework of three-dimensional configurational-forcedriven brittle crack propagation. *Comput Methods Appl Mech Eng* 2009; 198(15): 1413–1428.
[34] Hill R. On constitutive macro-variables for heterogeneous solids at finite strain. *Proc R Soc London A* 1972; 326(1565): 131–147.